J|A|C|S
ARTICLES
Published on Web 06/10/2003

Formation, Structure, and Structural Properties of a New Filamentary Tubular Form: Hollow Conical-Helix of Graphitic Boron Nitride

Fang-Fang Xu,* Yoshio Bando, Renzhi Ma, Dmitri Golberg, Yubao Li, and Masanori Mitome

Contribution from the Advanced Materials Laboratory and Nanomaterials Laboratory, National Institute for Materials Science, 1-1 Namiki, Tsukuba, Ibaraki 305-0044, Japan

Received January 3, 2003; E-mail: xu.fangfang@nims.go.jp

Abstract: A novel tubular form of graphitic boron nitride (BN) displaying a hollow conical-helix was discovered. It was generated via wrapping a single beltlike filament according to the geometry of an Archimedes spiral. Cone apex angles of helical-conical nanotubes (HCNTs) were found to exhibit specific values, each of which refers to a certain coincidence site lattice. A unique structural property of HCNTs was observed, displaying the transformation of apex angles during the annealing process. The observed apex angles were reduced with decreasing annealing temperature, which is in accordance with an estimated HCNT strain energy decrease for a given tubular radius. It is suggested that the curvature and apex angle of a HCNT are determined by a sole dynamic element, that is, enthalpy (ΔH), whereas the HCNT disclination configuration changes through helical sliding of the filament.

Introduction

A graphitic-like filament may form various curved structures such as fullerenes, nanotubes, and cones. Among these, graphitic nanotube is perhaps the most intriguing nanomaterial that has been proven to possess unmatched physicochemical properties and remarkable application potential. Cylindrical C and boron nitride (BN) nanotubes are composed of graphene sheets parallel to the tube axis independent of its chirality.[1] By contrast, turbostratic nanofibers of C and BN exhibit abundant morphologies, for example, so-called jellyfish, backbone, herringbone, horsetail, and bamboo-like. The last two morphologies contain cone-shaped compartments, whereas the herringbone-like fibers are the solid cones.

It has been indicated that the apex angle (θ_{apex}) of a stacked (i.e., nonhelical) cone can only display a limited number of values, which are determined by the disclination angles (θ_D) of multiple n of 60° (where n is a positive integer between 1 and 5).[2] Theoretically, due to the higher stability of B−N bonds relative to B−B and N−N bonds, there is a further restriction for θ_D in "hat-stacked" BN cones, which thus show angles of 120° and 240° only.[3] However, for helical cones, the apex angles have a somewhat broad selection due to the introduction of an overlap angle (θ_{over}) in addition to the n60° disclination issue. The overlap angles are determined according to the criteria of forming high densities of coincidence lattice sites between overlapping layers;[2b,c] they were observed to be 13.2°, 21.8°, and 27.8° in overlapping *h*-BN platelets.[3,4]

Although curved filamentary nanostructures are fairly clear, their nucleation and growth mechanisms have not yet been well understood. Among the various formation models, the ring-stacking model[5] suggested creation of curved surfaces via the selective assembly of monocyclic rings. In the case of the conical shape, it has been found that a single polygon defect, for example, a two- to five-membered atomic ring, is sufficient to form a twisted nucleus followed by further lateral growth of hexagons.[2,4b] This could be the case for solid cone particles. In the case of conical-shaped bamboo-like fibers with round conical caps, several reports have claimed similar formation mechanisms relying on growth on the conical catalytic particles.[6,7] Thus, cone apex angles have been suggested to strongly depend on the shape of the catalytic templates.

In the present paper, the synthesis of novel BN HCNTs with high purity is reported. Helical-conical BN nanotubes having no caps were observed. Because no catalytic particles were detected at the bottom of the cones, a new formation mechanism is proposed.

(1) (a) Iijima, S. *Nature* **1991**, *354*, 56. (b) Chopra, N. G.; Luyken, R. J.; Cherrey, K.; Crespi, V. H.; Cohen, M. L.; Louie, S. G.; Zettle, A. *Science* **1995**, *269*, 966. (c) Loiseau, A.; Willaime, F.; Demoncy, N.; Hug, G.; Pascard, H. *Phys. Rev. Lett.* **1996**, *76*, 4737.
(2) (a) Double, D. D.; Hellawell, A. *Acta Metall.* **1974**, *22*, 481. (b) Amelinckx, S.; Luyten, W.; Krekels, T.; Van Tendeloo, G.; Van Landuyt, J. *J. Cryst. Growth* **1992**, *121*, 543. (c) Krishnan, A.; Dujardin, E.; Treacy, M. M. J.; Hugdahl, J.; Lynum, S.; Ebbesen, T. W. *Nature* **1997**, *388*, 451.
(3) Bourgeois, L.; Bando, Y.; Han, W. Q.; Sato, T. *Phys. Rev. B* **2000**, *61*, 7686.
(4) (a) Bourgeois, L.; Bando, Y.; Shinozaki, S.; Kurashima, K.; Sato, T. *Acta Crystallogr., Sect. A* **1999**, *55*, 168. (b) Bourgeois, L.; Bando, Y.; Kurashima, K.; Sato, T. *Philos. Mag. A* **2000**, *80*, 129.
(5) Wakabayashi, T.; Achiba, Y. *Chem. Phys. Lett.* **1992**, *190*, 465.
(6) (a) Chen, Y.; Chadderton, L. T.; Gerald, J. F.; Williams, J. S. *Appl. Phys. Lett.* **1999**, *74*, 2960. (b) Chadderton, L. T.; Chen, Y. *J. Cryst. Growth* **2002**, *240*, 164. (c) Gerald, J. F.; Chen, Y.; Conway, M. J. *Appl. Phys. A* **2003**, *76*, 107.
(7) (a) Blank, V. D.; Gorlova, I. G.; Hutchison, J. L.; Kiselev, N. A.; Ormont, A. B.; Polyakov, E. V.; Sloan, J.; Zakharov, D. N.; Zybtsev, S. G. *Carbon* **2000**, *38*, 1217. (b) Terrones, H.; Hayashi, T.; Munoz-Navia, M.; Terrones, M.; Kim, Y. A.; Grobert, N.; Kamalakaran, R.; Dorantes-Davila, J.; Escudero, R.; Dresselhaus, M. S.; Endo, M. *Chem. Phys. Lett.* **2001**, *343*, 241.

10.1021/ja030003m CCC: $25.00

Table 1. Products from Different Synthesis Conditions

specimen	B_2O_3:CNT (in weight)	heating/postheating temperature (°C)	products
SH1850	6:1	1850/−	BN particles
SH1700	6:1	1700/−	BN microworms
SL1800	6:1	1700/1800	BN particles
S1800	8:1	1700/1800	BN HCNTs
S1750	8:1	1700/1750	BN HCNTs

It should be particularly emphasized that the well-known bamboo-like fibers consist of cone fragments stacking above each other; this leads to a tubular form that is periodically segmented by bridges, that is, conical caps. By contrast, BN HCNTs described here are made of a single filamentary belt wrapped conically and helically, which thus displays a continuous inner channel without segments, resulting in a real tubular morphology similar to C nanotubes.[1] The hollow helical rather than tightly stacked morphology allows a filament slide under external stress and/or thermal treatments without structural collapse. This leads to an unmatched structural property of a BN HCNT filament, that is, transformation of its apex angle during simple annealing.

Experimental Section

Materials Preparation. BN HCNTs were synthesized by employing a synthetic route similar to that previously reported, which led to cylindrical BN nanotubes via a substitution reaction from C nanotube (CNT) templates by B_2O_3 in N_2 atmosphere.[8] However, a postheating process at a high temperature was additionally performed in the present synthesis. First, CNTs were prepared from the starting mixture of N_2 (99.999%), H_2 (99.999%), and CH_4 (99.9%) by a plasma-assisted chemical vapor deposition (CVD) onto a Ti plate sputtered by Co nanoparticles. The substrate temperature was approximately 500 °C during the deposition. The obtained CNT powder then underwent a redox reaction with B_2O_3 in N_2 atmosphere inside a cylinder graphite crucible in a high frequency (21 kHz) induction furnace JHF-VFX 110 QZ (JEOL). The B_2O_3 powder was put at the bottom of the crucible, while CNTs were mounted on a graphitic disk ~0.8 cm above the B_2O_3 powder. The material was first heated at ~1700 °C for 30 min. A postheating process at higher temperature (1750−1900 °C) was then performed over 60 min. The reaction chamber was finally cooled to room temperature within 90 min in flowing N_2. The main experimental parameters that influenced the structures of the resultant products were found to be starting compositions and heating/postheating temperatures. Therefore, syntheses with different experimental conditions have been performed as listed in Table 1.

Annealing Processes. Annealing was performed to examine the specific structural properties of BN HCNTs. After being postheated at 1800 °C over 60 min, as described above (for specimen S1800, see Table 1), the material underwent an annealing process at a lower temperature in Ar atmosphere over 30 min. Two annealing temperatures (1700 and 1600 °C) were chosen in this study.

Structural and Chemical Analysis. The X-ray diffraction (XRD) data were collected by a powder diffractometer (Rigaku Rint 2000S) with graphite-monochromatized Cu Kα radiation ($\lambda = 0.15405$ nm). The microstructural analysis including measurement of apex angles was taken on a scanning electron microscope (SEM, JSM-6700F) and a 300 kV field-emission transmission electron microscope (TEM, JEOL-3000F). Chemical composition and elemental maps were acquired by using electron energy loss spectra (EELS) on a Gatan DigiPEELS 766 parallel detection spectrometer and an Omega filter JEOL-3100FEF transmission electron microscope, respectively. Carbon tetrachloride

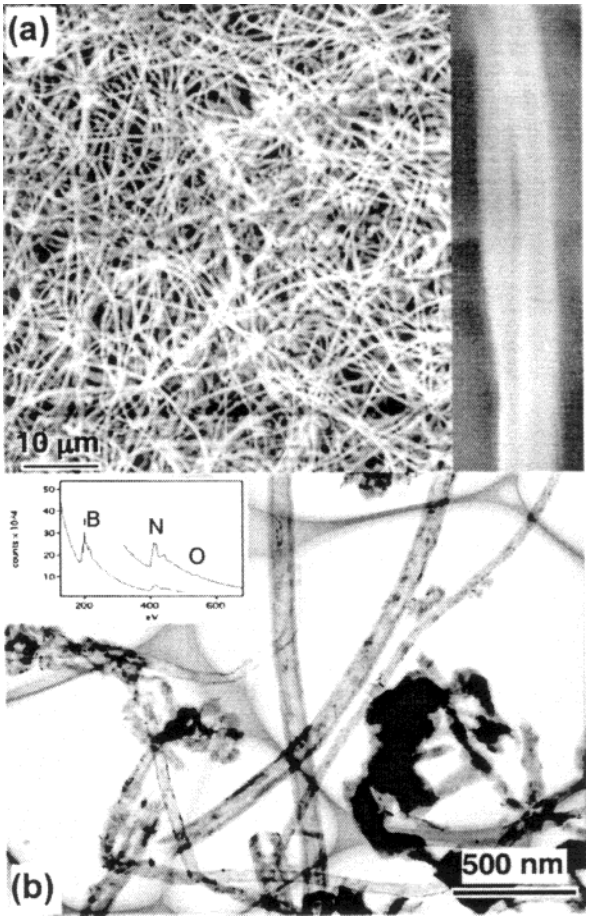

Figure 1. SEM (a) and TEM (b) images of BN HCNTs in the S1800 specimen. Inset in (b) shows a typical EEL spectrum of the material.

CCl_4 (>99.99%) was used during TEM specimen ultrasonic treatment followed by deposition on a standard C-coated-Cu TEM grid.

Results and Discussion

Structural Characterization. Table 1 indicates that only specimens S1800 and S1750 contain BN HCNTs. The SEM image (Figure 1a, for the specimen S1800 as an example) illustrates isomorphic one-dimensional nanostructures exhibiting a very high aspect ratio (~1000). An enlarged SEM image (inset of Figure 1a) and a TEM micrograph (Figure 1b) show clearly a tubular morphology. XRD and chemical analysis by EELS (inset in Figure 1b) reveal a pure graphite-like BN phase with the lattice parameters of $a = 0.2502$ nm and $c = 0.3333$ nm. Opposite from straight cylindrical BN nanotubes, typically displaying a length of several micrometers,[1c] the present nanostructures exhibit much higher length and bending curvature. The average length of BN nanotubes exceeds 100 μm, and the tubular radius ranges from 30 to 170 nm for the S1800 specimen, for instance. The lattice image (Figure 2a and b) displays oblique fringes (peculiar to graphene planes) with respect to the tube axis. This, along with the typical electron diffraction pattern (Figure 2c), which is characteristic of a conical geometry,[4] gives evidence of a hollow cone structure. The diffraction pattern consists of two rows of 00*l* reflections meeting at an angle equal to $180° - \theta_{apex}$ and *hk*0 arcs along the direction perpendicular to the cone axis.

Blank et al.[7a] and Terrones et al.[7b] have observed open graphitic cones forming on the conical catalytic particles. They

(8) Han, W. Q.; Bando, Y.; Kurashima, K.; Sato, T. *Appl. Phys. Lett.* **1998**, *73*, 3085.

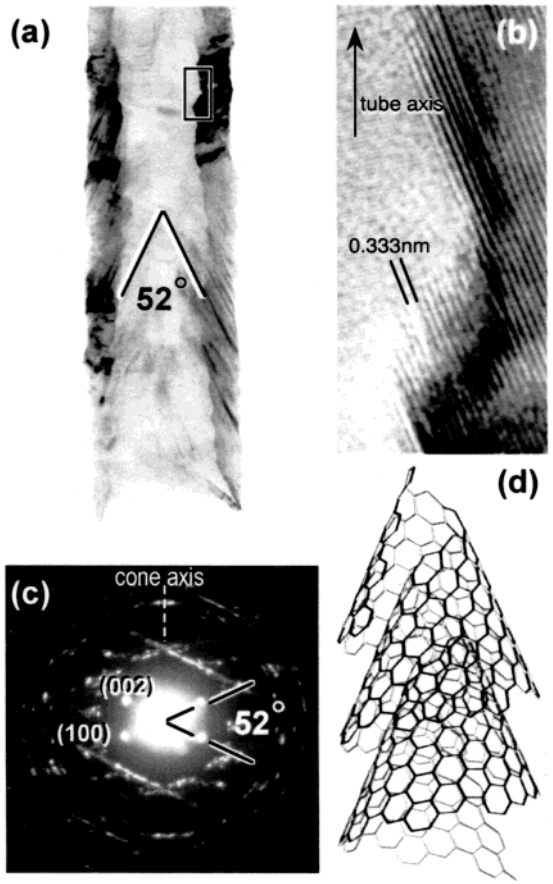

Figure 2. High-magnified image (a) of an individual BN HCNT in the S1800 specimen and the lattice image (b) of the framed region in (a) showing graphitic-like planes which are oblique to the tube axis. (c) and (d) are a diffraction pattern and a structural model of the present BN HCNT.

Table 2. Average Radii and Apex Angles in Different Specimens

	R_{av} (nm)		θ_{apex} (deg)		
specimen	range	peaked	range	peaked	peaked θ_D (deg)
S1800	30−170	60−100	43−60	52	180 + 21.8
S1750	70−200	110−150	35−71	46	240 − 21.8
SA1700	100−300	170−210	30−72	35	240 + 13.2
SA1600	130−320	200−240	19−46	30	240 + 27.8

characterized the cones as a stacked-type conical structure exhibiting certain limitations with respect to its apex angle. Our measurements of cone apex angles on the present BN conical filaments indicate a helical structure rather than a stacked type. Apex angles and average tubular radii R_{av} ($R_{av} = (R_{in} + R_{ex})/2$, where R_{in} and R_{ex} represent interior and exterior tubular radii, respectively), of about 30 BN nanotubes were measured for both S1800 and S1750 specimens and are summarized in Table 2. The measurements of apex angles were carried out on diffraction patterns if the cone axis was roughly perpendicular to the incident beam direction;[4a] the measurement uncertainty stands at 1°. The diagram shown in Figure 3 depicts the distribution of the apex angles. They were found to display some specific values within a narrow range rather than be randomly distributed. Moreover, each apex angle coincides with the theoretical value corresponding to a certain disclination configuration.[2,9] It is seen from Figure 3 that the majority of disclination angles includes a θ_{over} in addition to $n60°$, allowing us to conclude that the present BN nanotubes are formed via wrapping a narrow BN filamentary belt helically and conically rather than through packing of monolayer cones (for $\theta_D = n60$), as is schematically illustrated in Figure 2d. Thus, a novel tubular form is obtained displaying a geometry of a hollow conical-helix or Archimedes spiral. The observed disclination angles at 180° and 240° may refer to either a helical or a nonhelical cone structure, which could not be distinguished by any of the available techniques. For the present BN HCNTs, only $\theta_{over} = 21.8°$, 27.8°, and 13.2° were observed. These three values correspond to three coincidence site lattices (CSLs) with lattice parameters of $\sqrt{7}$, $\sqrt{13}$, and $\sqrt{19}\cdot a_0$ (a_0 refers to the in-plane dimension of *h*-BN unit cell), respectively.[9] They are the three smallest CSLs, indicative of an actual configuration with high densities of coincidence lattice sites between overlapping layers.

While CSLs and θ_{over} show well-defined configurations, the magnitudes of apex angles and radius, that is, the overall bending curvature, vary; the values and distribution are determined by the temperature. Table 2 displays the increase of an average radius, and hence decrease in overall bending curvature, when the synthesis temperature is decreased. However, apex angles change synchronically with temperature. Figure 3 demonstrates that these values for the S1800 specimen are centered at the higher apex angle, that is, 52°, whereas the distribution peak moves toward a smaller value ($\theta_{apex} = 46°$) for the S1750 specimen (synthesized at lower temperature). The two peaked apex angles are peculiar to the disclination angles of 180 + 21.8° and 240 − 21.8°, respectively. It appears that a small apex angle is energetically more favorable. This particular structural phenomenon will be further documented by an annealing process described later. It is noted that a hollow channel of conical tubes allows the cone axis not necessarily to be the tube axis; this explains a curved morphology of a rigid-bonded BN structure even if no C impurities and/or topological defects are introduced in it. The C impurities, which were always present in the BN nanotubes prepared via substitution from CNTs, were found at negligible levels in the present HCNTs, implying a different formation mechanism.

Formation Mechanism. It can be seen from Table 1 that BN HCNTs could only be observed in specimens S1800 and S1750, which were prepared using a significant excess of B_2O_3 in the starting powder mixture (high B_2O_3/CNTs ratios, see Table 1) and higher postheating temperatures. Synthesis without the postheating process at 1500−1850 °C has led to either cylindrical BN nanotubes[10] or nanofibers, or BN particles. Reaction at 1700 °C was found to form a new BN microstructure, as shown in Figure 4a, which displays a morphology similar to the bamboo-like fibers but with a uniform wall thickness and curvature, and a short spacing between neighboring compartments. These "wormlike" BN microfibers are found to play a crucial role in the formation of BN HCNTs. The curved surfaces of "microworms" behaved as templates for nucleation and growth of HCNTs, as is evidenced in Figure 4b. Therefore, the formation of BN HCNTs can be described by the following reactions.

At 1700 °C (for heating):

$$3C\ (\text{nanotubes}) + 2B_2O_3 + 2N_2 \rightarrow 4BN\ (\text{microworms}) + 3CO_2 \quad (1)$$

(9) Xu, F. F.; Bando, Y. *Acta Crystallogr., Sect. A* **2003**, *59*, 168.
(10) Bando, Y.; Ogawa, K.; Golberg, D. *Chem. Phys. Lett.* **2001**, *347*, 349.

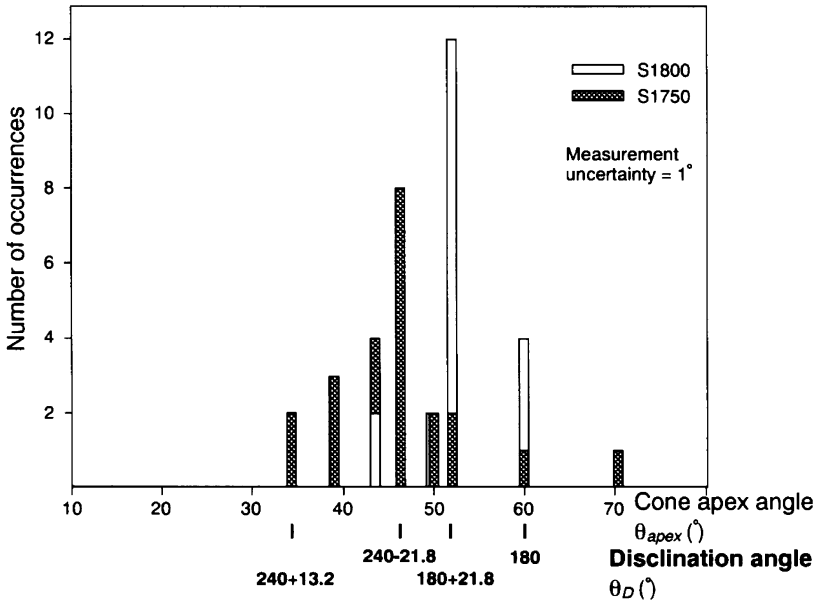

Figure 3. Distribution of the apex angles in the specimens S1800 and S1750. The corresponding disclination angles are indicated.

At 1750 or 1800 °C (for postheating):

$$B_2O_3 + C\ (\text{crucible}) \rightarrow 2BO + CO \quad (2)$$

$$B_2O_3 + 3CO + N_2 \rightarrow 2BN\ (\text{HCNT}) + 3CO_2 \quad (3)$$

$$6BO + N_2 \rightarrow 2B_2O_3 + 2BN\ (\text{HCNT}) \quad (4)$$

$$BN\ (\text{microworms}) \rightarrow BN\ (\text{particles}) \quad (5)$$

CNTs have been proven to be the templates and reduction reagents for the formation of BN nanostructures at the initial reaction stage.[11] Because all CNTs have been consumed during the formation of BN phases at the first heating stage, as confirmed by the chemical analysis of the specimen SH1700, the reduction reagent for the reactions in the postheating process appears along with reaction 2; that is, CO vapor originates from the graphite crucible used. Thus, CNTs played no role in the formation of nanostructures at the postheating stage. The possible contribution of metal particles to the nucleation of conical nanotubes, as observed in bamboo-like nanofibers by several authors,[6,7] may also be ruled out due to the fact that no Co crystallites were ever found at tube ends. On the other hand, the curved surfaces of the microworms could be responsible for the formation of conical graphitic sheets rather than cylindrical tubules (see Figure 4b). Because fewer BN microworms were observed in the final HCNT specimens, most of the thin microworms have eventually been collapsed and converted to particles at the later stage of postheating at temperatures over 1750 °C (see reaction 5). Numerous nucleation sites on the surface of microworms led to a high yield of HCNTs, while postheating at a certain high temperature and hence the high B_2O_3 or BO vapor pressure guarantees the fast formation of a uniform structure. It turns out that packing of BN layers is more favorable and thus proceeds faster than continuous growth of an individual BN graphitic-like sheet. This postulate is in accordance with the rare occurrence of single-wall BN nanotubes and the fact that typical BN nanotubes are usually short.[1c] Helical wrapping of a BN thin belt favors the packing growth mode of graphene sheets and hence faster growth of HCNTs and consequently extreme high aspect ratios. Meanwhile, the high temperature provides energetic support for the formation of the conical structure.

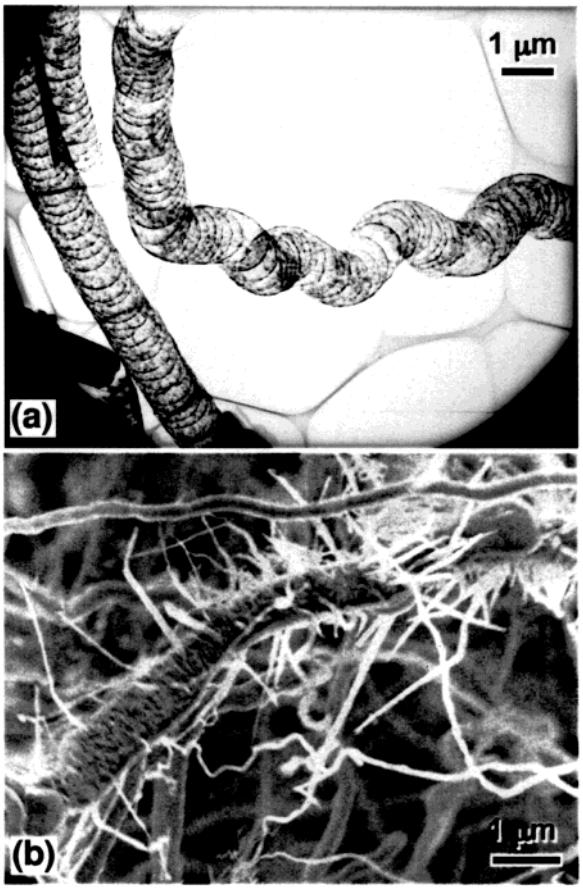

Figure 4. (a) TEM image of BN microworms in the SH1700 specimen. (b) SEM image of an individual BN microworm (in S1750) on which HCNTs have been nucleated.

(11) Golberg, D.; Bando, Y.; Kurashima, K.; Sato, T. *Chem. Phys. Lett.* **2000**, *323*, 185.

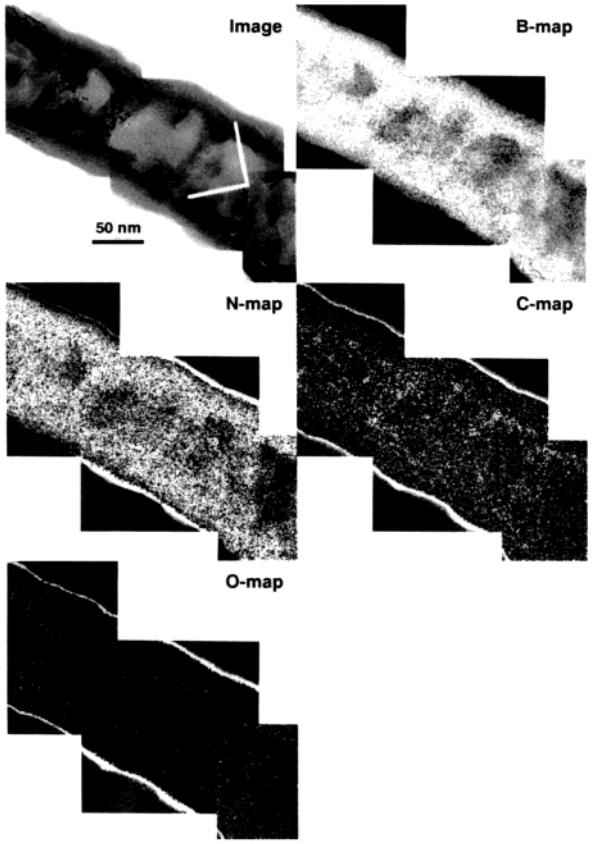

Figure 5. Bright-field image of an individual HCNT and its elemental maps that were obtained using energy-loss edges of B−K, N−K, C−K, and O−K, respectively. The apical direction is indicated on the bright-field image.

It has been indicated that an enthalpy (ΔH) is the driving force for the formation of curved structures while an entropy (ΔS) plays a dominating role in the distribution of disclinations formed.[2c] In some previous nucleation and growth models, a disclination configuration is determined during the nucleation stage and does not change after seeding.[2] However, the absence of apexes and catalytic particle at the tube ends, along with the narrow distribution of apex angles and hence disclination angles, as observed in BN HCNTs, contradicts the dominant role of the entropy in the present case. The S1800 and S1750 specimens postheated at different temperatures show a different distribution of apex angles, although they had experienced the same heating temperature (1700 °C) at which microworms were actually formed. This excludes the possible dependence of final apex angles on the curvature of microworms. These results imply changes of disclination configuration during the postheating process, which transforms the apex angles to a stable value determined by the temperatures. Thus, the single enthalpy factor determines the final disclination configuration of HCNTs.

A hollow conical-helix is actually not formed soon after the nucleation of a wrapping cone on the microworm. Numbers of bridges were formed along the tube axis segmenting the hollow chamber, showing a typical bamboo-like morphology (see Figure 5). A phenomenon that should be noted is that the bridges were completely removed in the right-hand part of the tube, whereas they are only broken in the left-hand region. EELS elemental mapping (Figure 5) shows carbon and a trace amount of oxygen covering the interior surfaces of the tubes and surfaces on both sides of the broken bridges. The sharp bright contrast

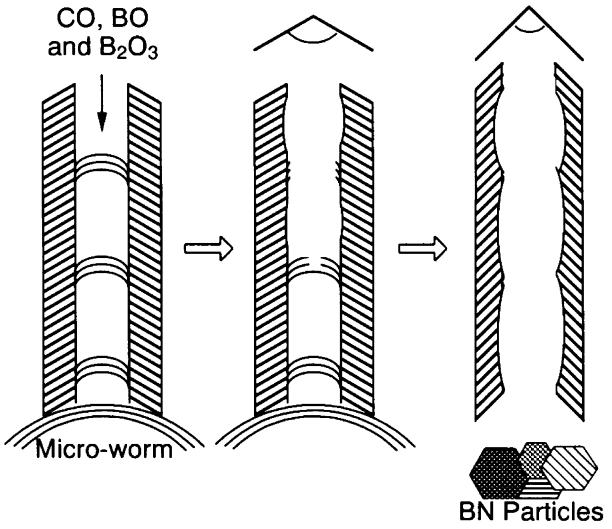

Figure 6. Schematic presentation of the formation mechanism for the present HCNTs, exhibiting elimination of interior bridges via a chemical reaction, which eventually led to a tubular morphology. A final stable apex angle is determined by temperature and has been achieved via the slide of filaments after microworms were collapsed and converted to particles.

appearing along the exterior surface in Figure 5 is an optical artifact, not referring to segregation of a certain element. It is obvious that the chemical reaction occurred inside of the tubes, which destroyed the bridges. In Figure 5, it looks that the reaction took place from the right-hand open end of the tube. By noting the direction of the apex, we found that the morphology suggests that chemical erosion starts from the open cap at the conical apical region; this implies that the bottom of the tube is sealed. The reactants, either CO or BO, flew along the tubular channel through its open cap. This phenomenon coincides with the nucleation of HCNTs on the surface of microworms. The formation mechanism can then be clarified as is schematically illustrated in Figure 6. It is possible that the nucleation of HCNTs on the surface of microworms employs a disclination configuration depending on the curvature of the microworms and the size of the cones. The absence of polygon defects results in conical fragment appearance rather than fullerene-type shells packed onto the curved surface of microworms. However, high temperature postheating destroyed microworms, resulting in isolated HCNTs which further undergo reconstruction of disclination configuration, governed by temperature. Change of disclination configuration, and hence the apex angle, has been observed recently during the deformation process of HCNTs.[12] Reconstruction is achieved via helical sliding of filaments. Apart from an external stress, thermal treatment is also found to ensure a driving force for the reconstruction, as is evidenced by the annealing process described below.

The round morphology of bridges inside the initial HCNTs requires the introduction of a considerable amount of topological defects, for example, four- or five-membered rings depending on the curvature. For the binary BN system, odd-numbered rings imply the introduction of B−B or N−N bonds which are less favorable than B−N bonds under energetic consideration. The chemical reaction easily proceeds at these defect sites. The surface of a hollow conical-helix consists of filament edges,

(12) Xu, F. F.; Bando, Y.; Golberg, D.; Ma, R. Z.; Tang, C. C. *J. Chem. Phys.*, accepted.

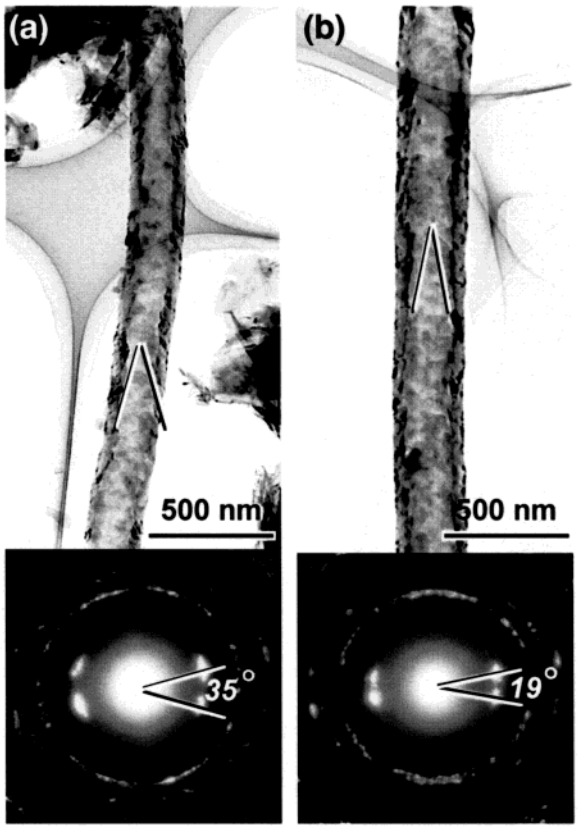

Figure 7. TEM image and diffraction pattern of an individual HCNT in the specimens SA1700 (a) and SA1600 (b), which have experienced annealing at 1700 and 1600 °C, respectively.

leaving B and N atomic bonds unsaturated. Reactants are then absorbed on the interior surface. At present, it is not fully clear whether the chemical reaction takes place on the interior or exterior surfaces of the tubes, leading to thinning of the tubular walls. Anyhow, the fact that almost all of the BN HCNTs display a flat exterior surface but a rough interior surface implies that the interior region is more reactive than the exterior one, as revealed by the EELS mapping. Thus, we suggest that some specific conditions for the dominant chemical reaction inside the nanoscaled HCNT channel are present.

Structural Properties. The above-mentioned chemical and structural examinations indicate that cone apex angles of HCNTs are determined by a sole dynamic element, enthalpy. The reconstruction of disclination configuration after the postnucleation stage is thus achieved through sliding of filaments. This phenomenon implies an interesting structural property of HCNTs, which may display a change in apex angles during annealing. In other words, we can control the apex angle, the most pronounced structural parameter for the present conical geometry. Therefore, annealing processes at two different decreased temperatures (1700 and 1600 °C) were employed. Systematic TEM observations did reveal a simultaneous reduction of apex angles but an increase in tubular radius. Figure 7a and b shows the typical morphologies and diffraction patterns of HCNTs annealed at 1700 (specimen SA1700) and 1600 °C (specimen SA1600), respectively. The measured apex angles and R_{av} in SA1700 and SA1600 are summarized in Table 2. Figure 8a illustrates the distribution of apex angles in SA1700 and SA1600, and Figure 8b compares the distribution of R_{av} in S1800 and SA1700. As compared to those in S1750, apex angles further decrease along with a decrease in annealing temperatures. The peaked apex angle tends to be 35° and 30° for specimens SA1700 and SA1600, respectively. The smallest apex angle was observed in SA1600, displaying a value of 19°, that is, corresponding to the highest disclination angle of 300°. It is indicated that the reconstructed conical configuration after annealing also employs ordered stacking modes showing specific values of θ_{over}.

During deformation of HCNTs, we observed that tension and/or torsion may cause the apex angle decrease along with a simultaneous decrease in tubular radius, leading to an increase of strain energy.[12] However, the present thermodynamic phenomenon which shows a decrease of the apex angle at lower temperatures does not suggest an increase in strain energy which, on the other hand, is determined by the overall bending curvature. The overall bending curvature is fully determined by the average tubular radius, R_{av}. A notable increase in R_{av}, and hence decrease in the overall bending curvature, was observed for specimens prepared at lower temperatures (see Table 2). S1800 has the smallest R_{av}, with a distribution centered around 60−100 nm, whereas the largest diameters R_{av} (up to 320 nm) were observed in SA1600 with a peaked value at 200−240 nm. Anyhow, systematic reduction of apex angles with a decrease in annealing temperatures is of great importance because it implies that such an important structural parameter can be controlled. It may be suggested that the reduction of apex angles under annealing at low temperatures is favored in terms of strain energy as described below.

On the basis of a continuum elastic model, Tibbetts[13] and then Robertson et al.[14] pointed out that the strain energy of an individual atom in a curved filament should increase inversely proportional to the square of the radius of curvature.

$$\sigma_i = \lambda R_i^{-2} \tag{6}$$

where R_i is the radius of curvature, and λ is a constant determined by the elastic modulus, filamentary structure, and atomic size. The strain energy (σ) for a cone can then be regarded as the sum of σ_i for all atoms with a linear change of R_i.

$$\sigma = \sum \sigma_i = \sum \lambda Ri^{-2} \tag{7}$$

or

$$\sigma = \rho \int_{R_{in}}^{R_{ex}} \lambda R^{-2} = \rho\lambda \frac{\Delta R}{R_{in} R_{ex}} \tag{8}$$

$$\Delta R = R_{ex} - R_{in} = L \sin(\theta_{apex}/2) \tag{9}$$

where ρ is a constant related to the number of atoms per area on a filament, and L is the generatrix of the cone. For a given average tubular radius, that is, R_{av} is a constant, the strain energy is solely dependent on θ_{apex} and gives

$$\sigma = \rho\lambda \frac{4L \sin(\theta_{apex}/2)}{4R_{av}^{\,2} - L^2 \sin^2(\theta_{apex}/2)} \qquad (0 < \theta_{apex}/2 < \pi/2) \tag{10}$$

(13) Tibbetts, G. G. *J. Cryst. Growth* **1984**, *66*, 632.
(14) Robertson, D. H.; Brenner, D. W.; Mintmire, J. W. *Phys. Rev. B* **1992**, *45*, 12592.

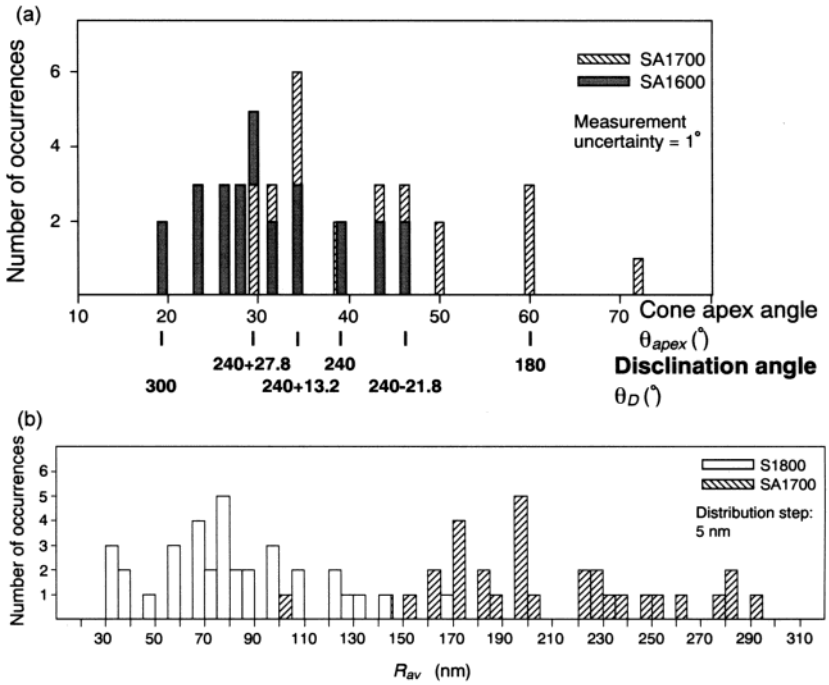

Figure 8. (a) Distribution of apex angles in the SA1700 and SA1600 specimens, and (b) distribution of R_{av} in the S1800 and SA1700 specimens.

We then obtain

$$\frac{\partial\sigma}{\partial(\sin(\theta_{apex}/2))} = \rho\lambda\frac{16R_{av}{}^2L + 4L^3\sin^2(\theta_{apex}/2)}{(4R_{av}{}^2 - L^2\sin^2(\theta_{apex}/2))^2} \quad (11)$$

It is noted that eq 11 gives a positive value, indicative of a synchronous change of strain energy with apex angle. Thus, a small θ_{apex} is energetically more favorable for a given R_{av}. It is noted that a large apex angle refers to a large curvature difference (characterized by $\sin(\theta_{apex}/2)$) on the curved filament. The large curvature difference implies that higher density and a larger variety of distorted bonds in the structure, leading to the lack of structural rigidity, periodicity, and continuity, and higher strain energy are involved, and thus it is less stable. Only enthalpy can provide energetic support for the formation of such a severely strained structure at the expense of crystal potential. Strain relaxation is achieved by decreasing the apex angles in addition to the increase in tubular radius. Reconstruction of the molecular structure can be performed via the sliding of filaments and, possibly, the skipping of atoms within a certain range, leading to a configuration with decreased overall bending curvature and a moderate curvature difference. The least strained curved geometry is expected to be achieved when $\theta_{apex}/2 = 0$, that is, for the conventional cylindrical nanotubes. This accounts for the fact that cylindrical BN nanotubes were usually obtained at relatively low temperatures, for example, 1200−1500 °C, while the higher temperatures (>1750 °C) generated conical structures.[4]

The specific geometry of the HCNTs is expected to exhibit some new properties and promising application potentials as compared to the cylindrical graphitic tubular form. The conical-helix allows the easy slide of filaments prior to bending and fracture. Actually, a novel deformation mechanism for HCNTs upon external stresses has been observed and will be reported elsewhere.[12] The tubes deform through changing the apex angles stepwise. Such deformation behavior results in the striking flexibility and elasticity of BN, which become comparable to those of metals. Keeping in mind the inherent high strength and outstanding chemical and thermal stability, we found that BN HCNTs exhibit, in some senses, apparent advantages over metal, polymer, and inorganic compound nanofibers and may become a key candidate for applications in high-performance composite materials for both low- and high-temperature usages. The presently observed structural property of the HCNTs suggests a possibility for controlling the apex angles artificially. Although the exact role of the apex angle for the HCNT physicochemical properties, for example, field emission, is not yet clear, the present discovery suggests an obvious practicability of the effect for controlling nanomaterial properties. Nevertheless, further theoretical and experimental work is required to investigate the role of apex angles for HCNT physiochemical properties.

Conclusion

We report on the synthesis and structural characterization of a novel graphitic tubular material displaying a hollow conical-helix geometry. A new formation mechanism is proposed and discussed in detail. A sole dynamic element, that is, enthalpy (ΔH) or postheating temperature, is found to determine the disclination configuration of HCNTs. The specific geometry of HCNTs leads to an interesting structural property, that is, transformation of apex angles under annealing. This implies the possibility of nanostructure design and control of its properties. The present HCNTs are expected to bring about new properties and applications in chemistry, physics, and materials science.

Acknowledgment. The authors thank Mrs. K. Kurashima and K. Fushimi for assistance in the experimental work.

JA030003M